Journal of Molecular Spectroscopy 255 (2009) 13–23

Contents lists available at ScienceDirect

Journal of Molecular Spectroscopy

journal homepage: www.elsevier.com/locate/jms

H_3^+ as the benchmark for rigorous *ab initio* theory

Christopher P. Morong [*,1], Jennifer L. Gottfried [2], Takeshi Oka

Departments of Chemistry, Astronomy & Astrophysics, The Enrico Fermi Institute, University of Chicago, Chicago, IL 60637, USA

ARTICLE INFO

Article history:
Received 22 October 2008
In revised form 30 January 2009
Available online 21 February 2009

ABSTRACT

The observed ro-vibrational spectral lines of the simplest polyatomic molecule, H_3^+, serve as the benchmark to test the most rigorous *ab initio* theory of intra-molecular dynamics. The ground state equilibrium structure of H_3^+ is an equilateral triangle, but near the energies of $\sim 9913\ cm^{-1}$, the so called barrier to linearity, it begins to sample linear configurations for which theoretical calculations are challenging because of the singularity of the Hamiltonian. We present here a continuation of the spectroscopy of H_3^+ above the barrier to linearity using a Ti:sapphire laser based high sensitivity spectrometer which allowed us to observe the spectrum with near shot-noise limited sensitivity. 121 new lines have been recorded from the near infrared $10300\ cm^{-1}$–$13700\ cm^{-1}$ entering the visible region bringing the total number of transitions above $10000\ cm^{-1}$ to 143. The observed spectrum is compared with theoretical predictions. The remaining discrepancies mostly due to vibrational and rotational non-adiabatic effects are discussed.

1. Introduction

Since the original work of Heitler and London [1] in 1927 and the extensive theoretical calculations by James and Coolidge [2,3] before the advent of electronic computers, spectroscopy of H_2, the simplest molecule, was the benchmark to test accurate *ab initio* molecular theory [4]. After many years of exchange between experimentalists and theorists (See Herzberg's review [5]), the theory reached a plateau in 1975 with the work of Kołos and Wolniewicz [6] which gave the dissociation energy and rovibrational energies of H_2, HD, D_2 to 'spectroscopic accuracy', that is within a fraction of a cm^{-1} of experimental values by Herzberg and colleagues [5]. Similar accuracy was reported by calculations of Bishop and Cheung [7] for HeH^+ in 1979 although there were no experimental results to compare with.

H_3^+ is the simplest polyatomic molecule and hence serves as the benchmark for rigorous *ab initio* theory. With two electrons like H_2, but with three protons instead of two, namely, with three inter-nuclear coordinates rather than one, the rigorous treatment for H_3^+ is much more demanding than for H_2. After its discovery by J.J. Thomson in 1911 [8], the divalent nature of bonding was a mystery to authors of early theoretical papers including illustrious names such as Bohr [9], Massey [10], Hirschfelder [11–15], and Eyring [12,13]. With Lennard–Jones's suggestion, Coulson [16] applied the molecular orbital method to H_3^+ and concluded that its equilibrium structure is an equilateral triangle although the calculation was severely criticized [12]. These pioneering papers were followed by a great many theoretical works especially after the advent of modern computers (see Oka [17], McNab [18] and Anderson [19] for review).

The new era of *ab initio* theory and spectroscopy of H_3^+ was initiated by two papers. Carney and Porter [20] published a milestone paper using variational methods not only for the calculation of potential energy surfaces (PES) but also for treating the motion of the three protons in the PES and predicted the first accurate vibrational frequencies and rotational constants taking into account the anharmonicity of vibration. In 1980, the infrared vibration–rotation spectrum of the ν_2 degenerate fundamental band was discovered in the laboratory [21]. Unlike the vibration–rotation spectrum of ordinary molecules, no apparent symmetry or regularity was noticed (hence Herzberg's remark "Who would have expected that this spectrum, ..., would be so complicated?" [5]) indicating an extraordinarily large vibration–rotation interaction and poor convergence of the orthodox perturbation treatment. The ℓ-doubling constant which is usually on the order of one-hundredth of the rotational constants is as large as $-5.38\ cm^{-1}$ [21]. Although the fundamental band was analyzed by Watson [22] using the traditional vibration–rotation theory based on the Wilson–Howard–Watson Hamiltonian, it was obvious that a paradigm shift was needed to analyze higher excited states of H_3^+.

The 1984 paper by Tennyson and Sutcliffe [23,24], which used a rigorous overall rovibrational Hamiltonian in Jacobi coordinates without separating vibration and rotation by the Eckart condition and solved its eigenvalue problem by the variational method, was the beginning. Subsequent extensive computational calculations by Miller and Tennyson [25–27] using this method and based

* Corresponding author.
E-mail addresses: cmorong@uchicago.edu (C.P. Morong), t-oka@uchicago.edu (T. Oka).
[1] Present address: Department of Geophysical Sciences, University of Chicago, Chicago, IL 60637, USA
[2] Present address: U.S. Army Research Laboratory, Aberdeen Proving Ground, MD 21005-5069, USA

0022-2852/$ - see front matter © 2009 Elsevier Inc. All rights reserved.
doi:10.1016/j.jms.2009.02.010

on the accurate PES of Meyer, Botschwina and Burton [28] initiated active exchanges between theorists and experimentalists. They played a crucial role in the assignment of the H_3^+ emission from Jupiter [29] and laboratory spectroscopy of hot [30], overtone [31], and forbidden bands [32]. The 1996 *tour de force* calculation by Neale, Miller and Tennyson (NMT) [33] of frequencies and intensities of three million transitions for energy levels up to 15 000 cm^{-1} with $J \leqslant 20$ based on an empirical PES adapted to laboratory data provided a useful table of theoretical spectral lines which has been used since. Other theoretical papers of note were the calculation of the $J = 0$ vibrational levels up to ~20 000 cm^{-1} by Whitnell and Light [34] using a hyperspherical coordinate system and a three dimensional discrete variable representation, and accurate calculations of rovibrational levels using hyperspherical coordinate and harmonics by Wolniewicz and Hinze [35].

Watson [36] developed an independent formalism based on the Eckart axis with the three internuclear distances as internal coordinates and, using PES adapted to ever increasing laboratory data, provided generations of spectroscopic tables which guided laboratory spectroscopists in the 1990s. The 895 observed transitions with energy levels below 10 000 cm^{-1} published in 17 experimental papers are compiled by Lindsay and McCall [37] and compared with Watson's calculation, which agrees well with experiment mostly to within 1 cm^{-1}.

The new development of rigorous theoretical spectroscopy without depending on laboratory data was initiated in 1998 by Cencek, Rychlewski, Jaquet and Kutzelnigg [38,39] who gave a PES with sub-microhartree accuracy (<0.2 cm^{-1}) taking into account both the adiabatic and relativistic effects of electrons. Polyansky and Tennyson [40] and Tennyson et al. [41] used the potential to give highly accurate calculations on H_3^+ and its deuterated species in which the effect of non-adiabatic corrections were also included. The potential was used in a most rigorous calculation using hyperspherical coordinates by Schiffels, Alijah and Hinze (SAH) [42,43]. There has been an independent work with spectroscopic accuracy by the Spanish school (see [44] and references therein).

In the mean time the laboratory experiments moved from the range of communication diodes (~8000 cm^{-1}) [45] to the titanium sapphire laser (~12 000 cm^{-1}) [46] and exceeded the barrier to linearity which is at ~9913 cm^{-1} [42] where the theoretical calculations become challenging because of the singularity of the rovibrational Hamiltonian. The observed spectrum agrees with the theoretical calculation which uses only natural constants and no empirical parameters mostly within 1 cm^{-1}. This situation of agreement between experiment and theory of H_3^+ may be likened to the state of H_2 in 1975 when the theory of Kołos and Wolniewicz [6] and Herzberg's experiment agreed to within 1 cm^{-1}. It took 30 years to make the progress from a two proton to a three proton problem with the enormous development of modern computers.

In this paper we report our H_3^+ spectroscopy which now entered the visible region with transitions up to 13 676 cm^{-1}. For such energies the deviations from theory are often more than 1 cm^{-1} and it gives further challenges to theorists. We also report observations of many weak lines whose observations were made possible by improving the sensitivity of our spectrometer to be nearly shot noise limited. Our measurements include high rotational lines up to $J = 6$. Such high J lines have high deviations from theory and are particularly challenging for theorists. These transitions are more than four orders of magnitude weaker than the fundamental. Since the shot noise limit is an absolute limit for photon counting spectroscopy, observations of higher energy overtone and combination bands is possible only by longer integration times.

Recently Kreckel et al. [47] applied the method of action spectroscopy developed by Schlemmer and Gerlich [48] up to 13 300 cm^{-1}. About 10^3 H_3^+ ions are stored in a radiofrequency ion trap to which Ar gas is introduced. The H_3^+ spectrum is recorded by counting ArH^+ ions which are generated when H_3^+ is pumped to a higher state by a titanium sapphire laser and the normally endothermic reaction, $H_3^+ + Ar \rightarrow H_2 + ArH^+$ becomes exothermic. This is a background free ion counting spectroscopy. Although limited to transitions starting from low J levels, this method is highly promising to take the H_3^+ spectroscopy deep into the visible and even ultraviolet as long as a sufficiently powerful laser is available to pump increasingly weaker transitions.

2. Assignments

The vibrational state of H_3^+ is defined in terms of the vibrational quantum number, v_1, for the totally symmetric breathing ν_1 mode and v_2 for the degenerate ν_2 mode. The doubly degenerate ν_2 vibrational mode has the added quantum number ℓ for the vibrational angular momentum which take on values $\ell = -v_2, -v_2 + 2, \ldots, v_2 - 2, v_2$. The rotational angular momentum k is the projection of the rotational angular momentum J along the C_3 symmetry axis. The vibrational angular momentum is highly coupled to the rotational angular momentum k through ℓ-resonance [21] making neither ℓ nor k good quantum numbers. A quantum number $g = k - \ell$ is a more robust quantum number and it is related to *ortho* and *para* H_3^+ in a rigorous way[49], i.e., $g = 3n$ for *ortho*-H_3^+ ($I = \frac{3}{2}$ where $\boldsymbol{I} = \boldsymbol{I_1} + \boldsymbol{I_2} + \boldsymbol{I_3}$) and $g = 3n \pm 1$ for *para*-H_3^+ ($I = \frac{1}{2}$). $G = |g|$ is a good quantum number at low energies but gets mixed at high energies. Each level is non-degenerate although g can be positive or negative. This is because only one of the two linear combinations $|g> \pm |-g>$ is allowed by the Pauli Principle; for the ground state it is $|k> - |-k>$. Since two k, ℓ combinations can often yield the same G, k and ℓ of the two levels are severely mixed and lead to an effect known as ℓ-resonance.

Observed transitions listed in Table 1 are labeled using the following convention [37]

$$v_1' v_1 + v_2' v_2^{|\ell'|} \leftarrow v_1'' v_1 + v_2'' v_2^{|\ell''|} \tag{1}$$

or it can be simplified as

$$v_1' v_2^{|\ell'|} \leftarrow v_1'' v_2^{|\ell''|} \tag{2}$$

where the double prime and prime denotes the lower and upper rovibrational states, respectively. Almost all transitions reported in this paper start from the ground vibrational state, that is, $v_1'' = v_2'' = \ell'' = 0$.

The convention set down by Lindsay and McCall [37] labels the rotational transitions as

$$^{[n|t|\pm 6|\pm 9|\ldots]}\{P|Q|R\}(J,G)^{[u|l]}_{[u|l]}, \tag{3}$$

where $\{P|Q|R\}$ represents the $\Delta J = \{-1|0|+1\}$, (J,G) are the values of J and G in the lower state, and $[u|l]$ discriminates between the two levels in an ℓ-resonance pair. The subscript (superscript) refers to the lower (upper) state in the transition. The index u refers to the upper energy level of the pair in the ℓ-resonance and the index l refers to the lower energy level. The left superscript represents the value of ΔG. For $\Delta G = 0$ which applies to most $\Delta\ell = \pm 1$ transitions, the superscript is omitted for brevity. For $\Delta G = -3$, and +3, n and t are used, respectively, and for larger ΔG values, the numerical value of ΔG is used. For the special case $\Delta G = +1$, which occurs because $g' = \pm 2 \leftarrow g'' = -(\pm)1$, $\Delta g = \pm 3$, n is used. $\Delta G = +2, +4$ can also exist from $g' = \pm 5 \leftarrow g'' = -(\pm)1$, and $g' = \pm 4 \leftarrow g'' = -(\pm)2$ both of which are $\Delta g = \pm 6$.

However not all the quantum numbers are defined in terms of pure integers. Only the parity and the total angular momentum F ($F = J + I$) are rigorous quantum numbers, although the rotational angular momentum, J, and the total nuclear spin angular momentum, I, are almost rigorous quantum numbers. On the contrary v_1,

Table 1
Observed transition frequencies and intensities of H_3^+.

Assignment	Band	Frequency (cm^{-1})	Int.[b]
$^tP(3,0)$	$2\nu_1+2\nu_2^2\leftarrow 0$	10322.235(10)	14.0
$R(6,6)$	Unknown	10329.307(10)	22.7
$^nR(2,2)$	$4\nu_2^4\leftarrow 0$	10366.546(10)	16.8
$^nR(2,1)$	$4\nu_2^4\leftarrow 0$	10367.184(10)	43.2
$^nR(3,3)$	$4\nu_2^4\leftarrow 0$	10454.539(10)	44.3
$P(6,6)$	Unknown	10462.405(10)	31.7
$^tQ(2,1)$	$2\nu_1+2\nu_2^2\leftarrow 0$	10467.800(10)	8.2
$^tQ(3,1)$	$2\nu_1+2\nu_2^2\leftarrow 0$	10468.544(10)	11.5
$R(5,5)$	Unknown	10496.287(10)	14.6
$^nP(2,1)$	$2\nu_1+2\nu_2^2\leftarrow 0$	10496.571(10)	6.3
$^tR(4,4)$	$2\nu_1+2\nu_2^2\leftarrow 0$	10497.078(10)	40.7
$^nP(3,2)$	$2\nu_1+2\nu_2^2\leftarrow 0$	10507.396(10)	6.6
$^nP(4,3)$	$2\nu_1+2\nu_2^2\leftarrow 0$	10528.992(10)	6.3
$^nP(5,5)^l$	$2\nu_1+2\nu_2^2\leftarrow 0$	10558.882(10)	42.9
$^tQ(3,0)$	$2\nu_1+2\nu_2^2\leftarrow 0$	10560.443(10)	31.8
$^tQ(1,0)$	$2\nu_1+2\nu_2^2\leftarrow 0$	10568.209(10)	30.1
$R(4,3)$	Unknown	10573.997(10)	23.9
$^nP(1,1)$	$2\nu_1+2\nu_2^2\leftarrow 0$	10581.256(10)	9.8
$^nP(3,3)$	$2\nu_1+2\nu_2^2\leftarrow 0$	10583.688(10)	27.0
$^nP(2,2)$	$2\nu_1+2\nu_2^2\leftarrow 0$	10586.424(10)	8.9
$^tR(3,3)$	$2\nu_1+2\nu_2^2\leftarrow 0$	10609.077(10)	27.6
$^tR(2,2)$	$2\nu_1+2\nu_2^2\leftarrow 0$	10621.634(10)	35.8
$P(4,3)$	$5\nu_2^1\leftarrow 0$	10624.888(10)	42.9
$P(4,4)$	$5\nu_2^1\leftarrow 0$	10632.042(10)	47.3
$Q(5,0)$	Unknown	10639.058(10)	15.3
$^tR(1,1)$	$2\nu_1+2\nu_2^2\leftarrow 0$	10641.024(10)	27.6
$^{+6}Q(3,0)$	$5\nu_2^3\leftarrow 0$	10657.149(10)	22.2
$Q(5,3)$	Unknown	10666.604(10)	20.2
$^nQ(1,1)$	$2\nu_1+2\nu_2^2\leftarrow 0$	10669.815(10)	15.0
$^nQ(2,1)$	$2\nu_1+2\nu_2^2\leftarrow 0$	10671.864(10)	8.8
$^nP(4,4)^u$	$2\nu_1+2\nu_2^2\leftarrow 0$	10686.611(10)	33.3
$^tR(4,3)$	$2\nu_1+2\nu_2^2\leftarrow 0$	10690.240(10)	25.2
$^tR(3,2)$	$2\nu_1+2\nu_2^2\leftarrow 0$	10705.364(10)	15.8
$P(3,2)$	$5\nu_2^1\leftarrow 0$	10705.894(10)	9.3
$Q(4,3)^u$	$5\nu_2^1\leftarrow 0$	10710.311(10)	48.6
$^tR(2,1)$	$2\nu_1+2\nu_2^2\leftarrow 0$	10725.953(10)[a]	18.1
$P(3,3)$	$5\nu_2^1\leftarrow 0$	10730.107(10)[a]	64.9
$^tR(1,0)$	$2\nu_1+2\nu_2^2\leftarrow 0$	10752.150(10)[a]	58.8
$P(2,2)$	$5\nu_2^1\leftarrow 0$	10752.369(10)[a]	31.2
$^nQ(3,2)^u$	$2\nu_1+2\nu_2^2\leftarrow 0$	10760.627(10)	4.1
$^nQ(2,2)$	$2\nu_1+2\nu_2^2\leftarrow 0$	10766.108(10)[a]	10.9
$P(2,1)$	$5\nu_2^1\leftarrow 0$	10766.320(10)[a]	13.0
$Q(3,2)^u$	$5\nu_2^1\leftarrow 0$	10779.136(10)[a]	13.6
$^{+6}Q(2,1)$	$5\nu_2^3\leftarrow 0$	10789.844(10)[a]	22.0
$^nQ(4,2)^u$	$2\nu_1+2\nu_2^2\leftarrow 0$	10793.060(10)	8.0
$P(3,0)$	$5\nu_2^1\leftarrow 0$	10798.691(10)	21.2
$P(1,1)$	$5\nu_2^1\leftarrow 0$	10798.785(10)	12.6
$^{+6}Q(3,1)$	$5\nu_2^3\leftarrow 0$	10803.820(10)	26.6
$^tR(3,1)$	$2\nu_1+2\nu_2^2\leftarrow 0$	10805.800(10)	10.7
$P(5,3)^l$	$5\nu_2^1\leftarrow 0$	10811.027(10)	15.8
$P(3,1)^u$	$5\nu_2^1\leftarrow 0$	10813.699(10)	11.6
$^{+6}Q(4,1)$	$5\nu_2^3\leftarrow 0$	10816.758(10)	15.5
$Q(1,0)$	$5\nu_2^1\leftarrow 0$	10831.677(10)	100
$^nR(1,1)$	$2\nu_1+2\nu_2^2\leftarrow 0$	10845.089(10)	12.1
$^nQ(4,3)$	$2\nu_1+2\nu_2^2\leftarrow 0$	10847.551(10)	16.0
$Q(4,2)^u$	$5\nu_2^1\leftarrow 0$	10855.172(10)	7.8
$P(6,6)$	$3\nu_1+\nu_2^1\leftarrow 0$	10874.681(10)	25.5
$^nR(2,1)$	$2\nu_1+2\nu_2^2\leftarrow 0$	10934.327(10)	14.9
$^tR(3,0)$	$2\nu_1+2\nu_2^2\leftarrow 0$	10935.358(10)	44.9
$Q(3,0)$	$5\nu_2^1\leftarrow 0$	10935.631(10)	53.7
$Q(1,1)$	$5\nu_2^1\leftarrow 0$	10939.559(10)	23.3
$P(5,5)$	$3\nu_1+\nu_2^1\leftarrow 0$	10953.026(10)	6.5
$^{+6}R(1,1)$	$5\nu_2^3\leftarrow 0$	10963.072(10)	10.3
$Q(2,2)$	$5\nu_2^1\leftarrow 0$	10964.605(10)	11.3
$^{+6}R(2,2)$	$5\nu_2^1\leftarrow 0$	10964.792(10)	6.3
$Q(3,3)$	$5\nu_2^1\leftarrow 0$	10968.257(10)	14.9
$P(4,3)$	$3\nu_1+\nu_2^1\leftarrow 0$	11015.488(10)	13.8
$^nR(2,2)^u$	$2\nu_1+2\nu_2^2\leftarrow 0$	11019.351(10)[a]	35.8
$^nR(3,1)^u$	$2\nu_1+2\nu_2^2\leftarrow 0$	11024.705(10)	4.9
$P(4,4)$	$3\nu_1+\nu_2^1\leftarrow 0$	11033.268(10)	16.1
$R(6,6)$	Unknown	11036.111(10)	23.1
$R(1,1)^l$	$5\nu_2^1\leftarrow 0$	11044.146(10)[a]	11.6
$R(5,5)$	Unknown	11046.569(10)	29.4
$R(4,4)$	Unknown	11048.996(10)	20.2
$R(3,3)^u$	$5\nu_2^1\leftarrow 0$	11053.686(10)[a]	90.2
$Q(2,1)^u$	$5\nu_2^1\leftarrow 0$	11071.117(10)	7.3
$P(3,3)$	$3\nu_1+\nu_2^1\leftarrow 0$	11111.798(10)[a]	19.9
$^nR(4,3)$	$2\nu_1+2\nu_2^0\leftarrow 0$	11114.428(10)	6.0
$R(5,0)$	Unknown	11114.628(10)	8.4
$R(3,2)^u$	$5\nu_2^1\leftarrow 0$	11195.625(10)	9.7
$R(1,0)$	$5\nu_2^1\leftarrow 0$	11228.601(10)[a]	82.4
$R(1,1)^u$	$5\nu_2^1\leftarrow 0$	11244.353(10)[a]	15.2
$R(2,1)^l$	$5\nu_2^1\leftarrow 0$	11246.707(10)[a]	17.9
$Q(3,0)$	$3\nu_1+\nu_2^1\leftarrow 0$	11278.517(10)	13.3
$R(2,2)^l$	$5\nu_2^1\leftarrow 0$	11304.480(10)[a]	18.8
$Q(1,0)$	$3\nu_1+\nu_2^1\leftarrow 0$	11318.080(10)[a]	15.5
$P(6,6)$	Unknown	11331.112(10)	14.9
$Q(3,3)$	$3\nu_1+\nu_2^1\leftarrow 0$	11358.855(10)	7.6
$^{-6}P(5,5)^u$	$5\nu_2^1\leftarrow 0$	11422.627(10)	6.9
$^{-6}P(4,4)$	$5\nu_2^3\leftarrow 0$	11482.938(10)	7.4
$P(4,3)$	$5\nu_2^5\leftarrow 0$	11496.203(10)	6.9
$P(3,3)$	$5\nu_2^3\leftarrow 0$	11496.055(10)	12.0
$R(2,1)^u$	$5\nu_2^1\leftarrow 0$	11496.796(10)[a]	16.7
$R(1,0)$	$3\nu_1+\nu_2^1\leftarrow 0$	11503.614(10)[a]	11.3
$^{+6}R(3,2)$	$5\nu_2^3\leftarrow 0$	11515.921(10)	16.3
$R(4,3)$	Unknown	11556.914(10)	35.7
$^tQ(3,0)$	$\nu_1+4\nu_2^0\leftarrow 0$	11562.798(10)	10.6
$^{+6}Q(3,1)$	$5\nu_2^5\leftarrow 0$	11564.098(10)	7.7
$P(3,3)$	$5\nu_2^5\leftarrow 0$	11571.876(10)[a]	20.5
$R(3,3)^l$	$5\nu_2^1\leftarrow 0$	11576.154(10)[a]	31.0
$^{+6}P(2,2)$	$5\nu_2^5\leftarrow 0$	11578.494(10)	18.7
$^{+6}Q(1,0)$	$5\nu_2^5\leftarrow 0$	11606.157(10)[a]	19.5
$R(3,0)$	$5\nu_2^1\leftarrow 0$	11618.521(10)	8.4
$R(3,3)^u$	$3\nu_1+\nu_2^1\leftarrow 0$	11668.916(10)	28.4
$Q(3,0)$	$5\nu_2^3\leftarrow 0$	11691.577(10)	8.2
$^{+6}R(2,2)$	$5\nu_2^5\leftarrow 0$	11694.789(10)[a]	9.5
$^{+6}R(1,1)$	$5\nu_2^5\leftarrow 0$	11707.268(10)[a]	8.9
$^{+6}Q(1,1)$	$5\nu_2^5\leftarrow 0$	11707.801(10)	6.1
$^{+6}R(3,1)$	$5\nu_2^5\leftarrow 0$	11728.382(10)	12.8
$Q(2,2)$	$5\nu_2^3\leftarrow 0$	11788.272(10)	5.1
$^{+6}R(3,2)$	$5\nu_2^5\leftarrow 0$	11793.656(10)	6.4
$^{+6}R(3,0)$	$5\nu_2^5\leftarrow 0$	11835.025(10)	15.7
$Q(3,3)$	$5\nu_2^5\leftarrow 0$	11839.565(10)	10.0
$^{+6}R(1,0)$	$5\nu_2^5\leftarrow 0$	11854.459(10)[a]	26.0
$^{-6}R(4,4)^l$	$3\nu_1+\nu_2^1\leftarrow 0$	11892.128(10)	7.1
$P(6,6)$	Unknown	11947.074(10)	5.0
$R(3,3)$	$5\nu_2^3\leftarrow 0$	11953.935(10)	9.4
$^tR(3,0)$	$\nu_1+4\nu_2^0\leftarrow 0$	11978.640(10)	8.6
$^nR(2,2)$	$\nu_1+4\nu_2^0\leftarrow 0$	12097.708(10)	8.4
$^tR(3,3)$	$\nu_1+4\nu_2^2\leftarrow 0$	12102.469(10)	2.0
$Q(3,0)$	Unknown	12116.353(10)	8.7
$^tP(4,3)$	$\nu_1+4\nu_2^4\leftarrow 0$	12181.941(10)	4.3
$Q(2,1)^l$	$2\nu_1+3\nu_2^1\leftarrow 0$	12207.905(10)	6.9
$P(2,2)$	$2\nu_1+3\nu_2^1\leftarrow 0$	12222.032(10)[a]	9.1
$^tR(1,0)$	$\nu_1+4\nu_2^2\leftarrow 0$	12246.368(10)[a]	7.1
$P(3,3)$	$2\nu_1+3\nu_2^1\leftarrow 0$	12246.574(10)[a]	15.5
$Q(1,0)$	$2\nu_1+3\nu_2^1\leftarrow 0$	12253.670(10)[a]	19.5
$^nQ(4,3)$	$\nu_1+4\nu_2^2\leftarrow 0$	12314.977(10)	6.8
$R(3,3)$	$5\nu_2^5\leftarrow 0$	12320.975(10)	6.7
$R(4,3)$	Unknown	12331.180(10)	7.8
$^tQ(1,0)$	$6\nu_2^2\leftarrow 0$	12419.140(10)[a]	14.2
$P(3,3)$	Unknown	12502.614(10)[a]	11.0
$^tQ(3,3)$	$\nu_1+4\nu_2^4\leftarrow 0$	12525.302(10)	11.5
$R(3,0)$	Unknown	12536.621(10)	6.8
$^tQ(1,1)$	$\nu_1+4\nu_2^4\leftarrow 0$	12623.171(10)	9.9
$^nR(3,3)$	$\nu_1+4\nu_2^2\leftarrow 0$	12658.335(10)[a]	24.1
$^tR(1,0)$	$\nu_1+4\nu_2^4\leftarrow 0$	12897.888(10)[a]	6.1
$R(1,0)$	Unknown	13056.013(10)[a]	13.8
$Q(1,0)$	Unknown	13597.367(10)[a]	5.1
$R(3,3)$	Unknown	13606.093(10)[a]	6.5
$Q(1,0)$	Unknown	13676.446(10)[a]	6.4
$R(2,0)$	Unknown$\leftarrow \nu_2^1$	10827.764(10)	1.9
$R(2,3)$	Unknown$\leftarrow \nu_2^1$	11265.189(10)	1.3

[a] Transitions reported in Gottfried[51].
[b] Measured intensities relative to $Q(1,0)$ of the $5\nu_2^1\leftarrow 0$ band which is taken to be equal to 100.

υ_2, ℓ and G undergo significant mixing with neighboring transition states. The amount of mixing was calculated by Watson [50] and is presented in Gottfried [51]. An important result from his calculations is that the mixed quantum numbers' expectation values tend

Table 2
Experimentally determined energy levels with assigned quantum numbers and calculated average quantum numbers.

v_1	$\langle v_1 \rangle$	v_2	$\langle v_2 \rangle$	ℓ	$\langle \ell \rangle$	G	$\langle G \rangle$	J	n	$\Gamma_{(rv)}$	u/l	E (cm^{-1})
0	0.094	4	3.910	4	3.605	1	1.221	3	36	E'		10535.843
0	0.079	4	3.923	4	3.702	2	2.068	3	27	E'		10604.538
2	2.000	2	2.000	2	2.000	2	2.000	0	9	E'		10645.377
2	1.998	2	2.003	−2	−1.998	3	2.993	1	9	A_2''		10655.167
2	1.988	2	2.015	−2	−1.990	4	3.958	2	29	E'		10705.150[a]
2	1.999	2	2.001	2	2.000	2	2.000	1	9	E'		10733.931[a]
2	1.998	2	2.003	2	1.991	1	1.004	1	21	E'		10755.721
0	0.145	4	3.862	4	3.304	0	0.798	4	18	A_2'		10769.885
2	1.952	2	2.053	−2	−1.961	5	4.853	3	38	E'		10790.931
2	1.992	2	2.014	−2	−1.997	3	2.982	2	9	A_2''		10839.112[a]
0	0.000	5	5.000	1	1.000	1	1.000	0	10	E'		10862.906
2	1.998	2	2.005	2	1.992	0	0.041	2	11	A_2'		10899.034
2	1.992	2	2.012	2	1.981	2	1.999	2	31	E'		10909.214[a]
0	0.002	5	4.996	1	1.010	0	0.014	1	10	A_2''		10918.635
0	0.003	5	4.993	−1	−1.275	2	2.003	1	22	E'		10921.666
2	1.769	2	2.237	−2	−1.829	6	5.335	4	19	A_2'		10924.423
2	1.996	2	2.005	2	1.937	1	1.006	2	21	E'		10935.410[a]
2	1.982	2	2.023	−2	−1.989	4	3.941	3	29	E'		10963.309[a]
2	—	2	—	2	—	7	—	5	52	E'		10999.111
0	0.002	5	4.998	1	1.001	1	1.001	1	10	E'		11003.677[a]
0	—	5	—	3	—	5	—	2	32	E'		11027.196[a]
0	0.008	5	4.983	−1	−1.036	3	3.001	2	12	A_2'		11045.453
2	1.982	2	2.024	−2	−1.973	3	2.967	3	21	A_2''		11077.324
0	0.012	5	4.978	1	1.412	1	1.034	2	33	E'	*l*	11108.267
2	1.937	2	2.069	−2	−1.958	5	4.812	4	38	E'		11133.383
0	0.003	5	4.994	1	1.642	2	2.003	2	22	E'		11133.908[a]
0	0.301	5	4.538	−1	−1.355	4	3.146	0	41	E'		11134.082[a]
2	1.980	2	2.028	2	1.905	2	1.998	3	31	E'		11171.681
0	—	5	—	3	—	6	—	3	22	A_2''		11174.030
2	1.955	2	2.063	2	1.499	0	0.105	3	19	A_2'		11187.707
2	1.979	2	2.028	2	1.234	1	1.081	3	42	E'	*u*	11188.646[a]
0	0.027	5	4.963	1	1.676	2	2.147	3	43	E'	*u*	11207.155
—	—	—	—	—	—	—	—	6	58	E'		11225.296
—	—	—	—	—	—	—	—	5	25	A_2'		11232.712
0	0.040	5	4.933	−1	−1.548	3	2.936	3	20	A_2'		11283.603[a]
2	1.912	2	2.117	2	1.946	2	2.149	4	51	E'	*l*	11287.891
0	—	5	—	3	—	5	—	3	32	E'		11298.586
2	1.948	2	2.073	−2	−1.978	4	3.857	4	52	E'		11300.566
0	0.028	5	4.962	1	1.284	1	1.032	2	34	E'	*u*	11308.470[a]
0	0.032	5	4.958	1	1.013	0	0.054	2	10	A_2''		11315.566[a]
—	—	—	—	—	—	—	—	7	30	A_2''		11325.177
2	1.620	2	2.398	−2	−1.997	6	4.812	5	26	A_2'		11348.955
0	0.051	5	4.912	1	1.206	3	3.178	4	21	A_2'	*u*	11369.029[a]
3	2.999	1	1.001	1	1.001	0	0.002	1	11	A_2''		11405.038
3	2.990	1	1.012	−1	−1.009	3	2.977	2	13	A_2'		11427.144
2	1.966	2	2.049	−2	−1.892	3	2.906	4	21	A_2''		11452.239
0	0.017	5	4.976	1	1.515	0	0.020	3	23	A_2''		11452.512
—	—	—	—	—	—	—	—	5	29	A_2''		11458.275
0	0.112	5	4.858	1	2.42	2	2.263	3	44	E'	*l*	11473.777
0	0.012	5	4.976	1	1.524	1	1.024	3	33	E'	*l*	11484.061
2	1.971	2	2.041	2	1.984	0	0.162	4	22	A_2'		11506.266
2	1.912	2	2.117	2	1.946	2	2.149	4	55	E'	*u*	11519.471
3	2.970	1	1.033	−1	−1.025	4	3.930	3	45	E'		11535.301
—	—	—	—	—	—	—	—	5	61	E'		11551.029
2	1.924	2	2.110	2	1.528	1	1.128	4	42	E'	*u*	11561.533
3	2.996	1	1.004	1	1.004	0	0.011	2	11	A_2''		11590.572
0	0.030	5	4.955	−1	−1.112	2	2.897	4	43	E'	*u*	11623.645[a]
0	—	5	—	3	—	5	—	4	56	E'		11650.338
3	2.987	1	1.013	−1	−1.006	3	2.968	3	21	A_2'		11674.202[a]
3	—	1	—	1	—	5	—	4	57	E'		11682.035
0	0.004	5	4.995	−5	−4.983	6	5.980	1	12	A_2''		11693.115
0	0.115	5	4.852	1	1.620	1	1.156	3	34	E'	*u*	11734.150
—	—	—	—	—	—	—	—	5	28	A_2'		11747.089
0	0.026	5	4.973	5	4.882	4	3.920	1	26	E'		11747.791
0	—	5	—	5	—	5	—	2	38	E'		11771.389
0	0.001	5	4.999	5	4.998	5	4.998	1	12	E'		11771.922
2	—	2	—	0	—	0	—	5	29	A_2'		11773.143
—	—	—	—	—	—	—	—	6	66	E'		11775.578
3	2.988	1	1.015	1	1.005	0	0.006	3	24	A_2''		11795.398
0	0.001	5	4.998	3	3.304	3	3.002	2	14	A_2'		11811.401
0	0.096	5	4.892	−5	−4.576	8	7.365	3	49	E'		11864.086
3	2.843	1	1.169	−1	−1.135	6	5.620	5	33	A_2''		11870.551
0	0.044	5	4.953	5	4.565	3	2.884	2	15	A_2'		11887.222
0	0.125	5	4.846	−1	−1.506	3	3.451	4	24	A_2'	*l*	11891.506[a]
—	—	—	—	—	—	—	—	5	34	A_2''		11910.322
0	0.071	5	4.925	−5	−4.794	6	5.790	2	12	A_2''		11941.417

Table 2 (*continued*)

v_1	$\langle v_1 \rangle$	v_2	$\langle v_2 \rangle$	ℓ	$\langle \ell \rangle$	G	$\langle G \rangle$	J	n	$\Gamma_{(rv)}$	u/l	E (cm^{-1})
0	–	5	–	3	–	4	–	4	45	E'		11943.940
0	0.015	5	4.983	3	2.975	2	2.007	2	26	E'		11957.569
3	2.964	1	1.042	−1	−1.032	3	3.020	4	25	A_2'	u	11984.262
0	0.099	5	4.891	3	3.157	2	2.012	3	50	E'		11984.971
–	–	–	–	–	–	–	–	7	36	A_2''		12031.981
0	–	5	–	5	–	5	–	3	38	E'		12058.864
1	–	4	–	0	–	3	–	3	26	A_2''		12079.679
0	–	5	–	1	–	0	–	4	23	A_2''		12135.402
0	0.447	5	4.511	1	1.205	1	1.368	4	61	E'	u	12151.636
0	–	5	–	5	–	3	–	3	23	A_2'		12154.915[a]
0	0.130	5	4.857	3	2.617	0	0.365	3	27	A_2''		12208.458
–	–	–	–	–	–	–	–	5	31	A_2'		12215.629
0	0.122	5	4.859	−5	−4.507	8	6.988	4	48	E'		12221.675
0	–	5	–	5	–	7	–	4	63	E'		12223.148
1	–	4	–	0	–	1	–	3	53	E'		12267.005
0	0.073	5	4.913	3	3.345	3	2.873	4	27	A_2'		12269.281
–	–	–	–	–	–	–	–	5	35	A_2''		12326.982
1	0.958	4	4.040	−2	−2.274	3	3.135	2	13	A_2''		12333.326
2	1.995	3	3.005	1	0.015	0	0.015	1	14	A_2''		12340.628
0	0.202	5	4.769	−5	−3.968	6	7.337	4	25	A_2''		12351.906
–	–	–	–	–	–	–	–	6	33	A_2''		12385.892
2	1.974	3	3.026	−1	−0.109	2	1.089	1	30	E'		12391.329
3	–	1	–	1	–	2	–	5	72	E'	l	12394.161
1	–	4	–	2	–	6	–	4	28	A_2'		12417.815
2	1.983	3	3.016	1	0.186	1	1.066	2	44	E'	l	12445.259
1	–	4	–	0	–	3	–	4	26	A_2''		12495.521
1	1.000	4	4.000	4	4.000	3	4.000	1	15	A_2''		12506.098
2	–	3	–	1	–	3	–	2	17	A_2'		12561.920
–	–	–	–	–	–	–	–	3	30	A_2''		12633.234
0	0.258	5	4.730	5	4.123	3	2.500	4	29	A_2'		12636.321
1	1.003	4	3.997	4	3.986	4	3.986	1	15	E'		12687.292
–	–	–	–	–	–	–	–	2	19	A_2'		12817.960
1	–	4	–	4	–	6	–	3	27	A_2'		12840.652[a]
–	–	–	–	–	–	–	–	5	41	A_2''		12942.944
1	–	4	–	2	–	0	–	4	32	A_2'		12973.687[a]
1	1.053	4	3.946	4	3.620	3	2.892	2	15	A_2''		12984.846
–	–	–	–	–	–	–	–	5	37	A_2'		12989.895
–	–	–	–	–	–	–	–	4	29	A_2''		13053.502
–	–	–	–	–	–	–	–	2	16	A_2''		13142.971
–	–	–	–	–	–	–	–	3	31	A_2'		13640.628
–	–	–	–	–	–	–	–	1	19	A_2''		13684.325
–	–	–	–	–	–	–	–	1	20	A_2''		13763.404
–	–	–	–	–	–	–	–	3	39	E'		13879.468
–	–	–	–	–	–	–	–	4	39	A_2'		13921.439

[a] Average value from two or three transitions.

to have nearly integer values even above the barrier to linearity for low values of J, but for high values of J the mixing becomes so severe that assigning an integer value would not be meaningful. Table 2 gives the best guess of the expectation values from the data Watson provided. In order to enumerate all rovibrational energy levels for a specific J value, the ordering index n is used which increases with energy. The ordering index, n, does not always agree between different authors and not all of the transitions could be unambiguously assigned, but it allows complete compilation of energy levels.

3. Experiment

Since intensities for the high transitions of H_3^+ considered here are more than four to five orders of magnitude weaker than the fundamental transition we need a high sensitivity spectrometer. The main experimental setup has been explained in detail in Gottfried et al. [46], but will be briefly outlined here in Fig. 1. A triple jacketed plasma discharge tube was used. The inner jacket contains the plasma and the outermost jacket is held under vacuum for thermal insulation. The middle jacket usually contains liquid nitrogen to produce rotational temperatures around 300 K for pure 500 mTorr H_2 discharges and 600 K for 10 Torr He plus 500 mTorr H_2 discharges. However to search for high J and hotband transitions, water cooling which produces rotational temperatures around 1000 K is used. The plasma is produced under several kV potential and run at 300 mA (rms) at 19 kHz. The AC discharge velocity modulates the ions, but does not velocity modulate neutrals. A very important exception is for metastable Rydberg states of hydrogen (H_2^*). H_2^* usually appear with an anionic signature (180° out of phase to the cations) because the formation process involves electron impact. The transitions are both strong and numerous and can completely swamp the much weaker H_3^+ signal. However by adding helium, we could reduce H_2^* by collisional quenching, without seriously affecting the H_3^+ signal. A particularly striking example is shown in Fig. 2. This is an unusually strong triplet H_2^* transition, $R(0)\ E^3\Sigma_u^+, v=2 \leftarrow A^3\Sigma_g^+, v=2$, corresponding to $3p\sigma \leftarrow 2s\sigma$. The strong Rydberg line is completely suppressed by the addition of 10 Torr He while the H_3^+ line does not change intensity appreciably. The Rydberg H_2^* lines sometimes occur as stimulated emission; in such a case the signal appears with a cationic signature [52].

A 10-W diode-pumped solid-state laser, Verdi-V10 (532 nm) pumps a Coherent 899-29 CW Ti:sapphire ring laser providing about 1 W of continuous power which produces a highly monochromatic radiation ($\Delta\nu\sim$ 500 kHz) which is continuously tunable

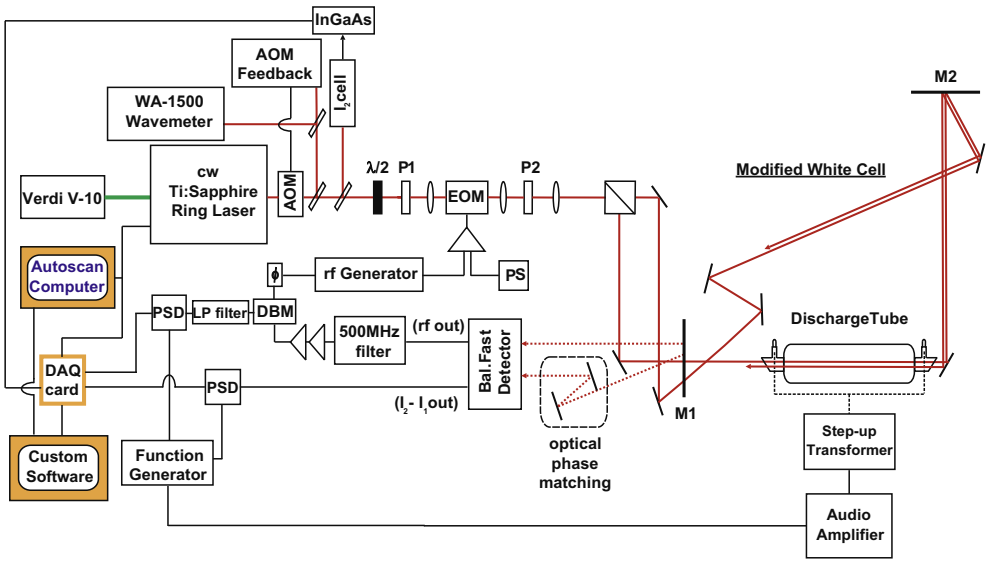

Fig. 1. Ti:Sapphire Laser Spectrometer. M1 and M2 refer to the mirrors in the modified white cell. P1 and P2 are Glan polarizers. PS is the power source to amplify the RF output. The DBM and LP Filter are the double balanced mixer and low pass filter respectively. PSD is the phase sensitive detector or lock-in amplifier. See text for additional details. Adapted from Gottfried et al. [46].

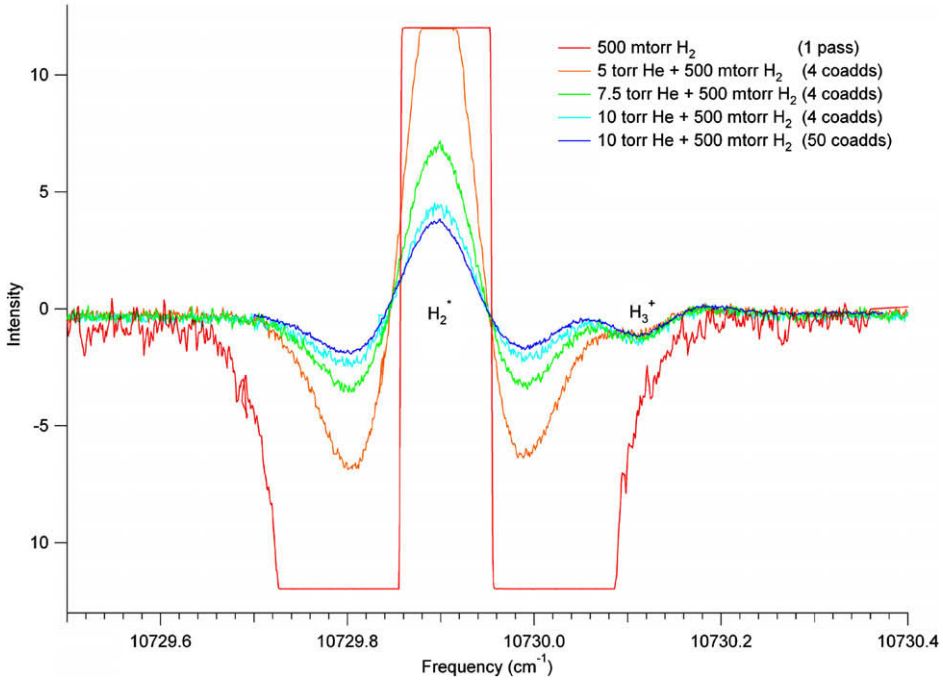

Fig. 2. Spectra of 500 mTorr of H_2 plus varying amounts of He between 0 and 10 Torr. While the signal of H_3^+ remains unaffected, the H_2^* signal is greatly diminished. This is a peculiarly strong Rydberg transition. Most are totally quenched with the addition of 10 Torr of He.

between 10300 and 14000 cm^{-1} through the use of three optics sets. For the atmospheric water absorptions between 10500 and 10700 cm^{-1} the laser cavity was purged with nitrogen to stabilize the laser power. Additionally a low power output coupler (0163-691-02) and intermediate fold mirror (0161-720-00) were used to increase the gain in the cavity and provide more stability and tunability. The laser intensity is controlled by an external acousto-optic modulator (AOM Isomet 1205C-2-NIR) which acts as an attenuator by feedback electronics. A pickoff of the main beam provides the reference for the AOM feedback, external wavemeter (Burleigh 1500-NIR) and heated iodine reference cell. A new computer control program interfaces the external wavemeter and the laser. The main beam passes through an electro-optic modulator (EOM) which phase modulates the light at 500 MHz. The modulation creates frequency sidebands at ±500 MHz the laser frequency. The beam is then split by a 50:50 beam splitter and one half travels unidirectionally four times clockwise and the other half four times counterclockwise via a modified White cell through the plasma cell yielding around 8 m of total pathlength. The two beams are detected by fast balanced photodiodes each of which takes a beat

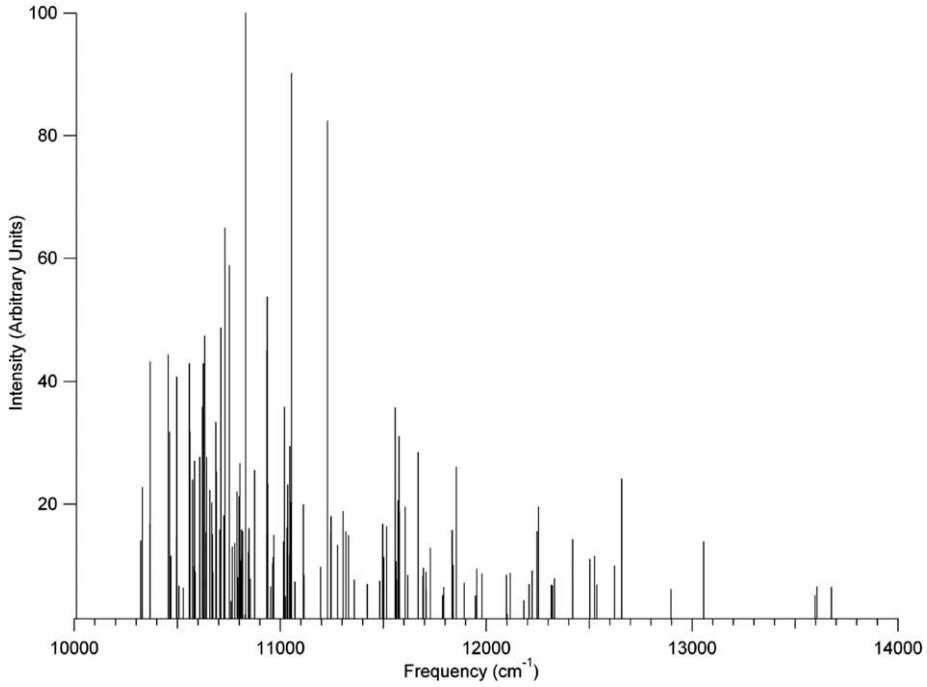

Fig. 3. Observed spectrum of H_3^+.

of 500 MHz between the carrier and the two sidebands. Since the phases of the two sidebands are opposite to each other, the beats cancel exactly if there is no absorption. An absorption causes unbalance between the beats and generates 500 MHz signal. The signal is amplified and demodulated using a double balanced mixer to complete the heterodyne detection. The velocity modulated signal is then demodulated at 19 kHz using a lock-in amplifier (PSD) referenced to the plasma frequency. The combination of the velocity modulation and phase modulation with heterodyne detection minimizes the effect of residual amplitude modulation and yields a second derivative Gaussian line shape and near shot noise limited sensitivity.

For most of the lines it took approximately one hour of integration over one wavenumber to obtain sufficient S/N for a conclusive identification. The weakest hotband transitions needed at least four hours of integration plus additional time to search several additional wavenumbers because of the larger theoretical errors.

4. Results

The observed transitions, assignments and relative intensities are given in Table 1 and shown in Fig. 3. The intensities are given relative to the $Q(1,0)$ transition of the $5\nu_2^1 \leftarrow 0$ band, the strongest transition in this spectral region. The rotational temperature of the plasma was 600 ± 30 K.

Since the recent theoretical predictions are generally within a wavenumber, assigning the transitions was straightforward when a line appears separated. In some cases when the lines appear close together theoretical intensity ratios were also used for the assignment. When possible, combination-differences in the lower state were used to establish the assignment. In cases when a H_2^* interfered, the pressure of the helium was changed to observe the response of the transitions. We have not seen any clearly visible H_3^+ spectral line which had not been predicted in the range of observation.

Since the energy values of the lower levels of the observed transitions are well known[37], observed frequencies listed in Table 1 give experimentally determined energy of the upper level. Their energy values relative to the $J = K = 0$ level, which is forbidden by the Pauli Principle and is 64.121 cm^{-1} below the $J = K = 1$ lowest level, are given in Table 2. Theoretical expectation values of quantum numbers $\langle v_1 \rangle$, $\langle v_2 \rangle$, $\langle \ell \rangle$, and $\langle G \rangle$ calculated by Watson, and the rotational angular momentum J, the ordering index n, and the symmetry of ro-vibronic wavefunction $\Gamma_{(rv)}$ are also given in the table. We use SAH's n value when the ordering index does not agree among different calculations.

5. Discussion

The observed frequencies of H_3^+ are compared with the theoretical values given by NMT [33] and SAH [42]. Differences between the observed and theoretical values are listed in Table 3. Since the agreement between the theory and experiment is very good for the ground state, these discrepancies are mostly due to discrepancies of the energy levels in the excited states. The three levels of theory for the SAH are separately given. $E^{(0)}$ is the result of the pure *ab initio* theory. After a comparison with the previously observed spectral lines below 9000 cm^{-1} [37], SAH noted a systematic deviation which could be expressed as [53].

$$E^{(2)} = E_{\mathrm{calc}} - b_1 E_{\mathrm{calc}}^{(0)} - \bar{a}_1 J(J+1) - \bar{a}_2 G^2 \tag{4}$$

where the empirical constants were found to be $b_1 = 1.0123 \times 10^{-4}$, $\bar{a}_1 = 2.0436 \times 10^{-3} \mathrm{cm}^{-1}$, and $\bar{a}_2 = -1.3600 \times 10^{-3} \mathrm{cm}^{-1}$. For highly mixed levels where quantum numbers J and G are not clearly identified, only the linear term is used

$$E^{(4)} = E_{\mathrm{calc}} - b_1 E_{\mathrm{calc}}^{(0)}. \tag{5}$$

These empirical correction terms are thought to be mostly due to non-adiabatic effects. The correction $-b_1 E_{\mathrm{calc}}^{(0)}$ which is the major term is due to vibrational non-adiabatic effects. This effect has been studies by Polyansky and Tennyson [40] and Tennyson et al. [41].

The correction involving rotational quantum numbers J and G are due to rotational non-adiabatic effect, that is, lagging of the electrons to the rotational nuclear motion which is related to pro-

Table 3
Comparison of observed frequencies with theoretical predictions of NMT and various level of SAH given as observed − calculated in cm^{-1}.

Assignment	Band	Observed (cm^{-1})	ΔNMT (cm^{-1})	ΔSAH $E^{(0)}$ (cm^{-1})	ΔSAH $E^{(4)}$ (cm^{-1})	ΔSAH $E^{(2)}$ (cm^{-1})
$^{n}R(2,2)$	$4\nu_2^4 \leftarrow 0$	10366.546	0.474	1.012	−0.038	−0.014
$^{n}R(2,1)$	$4\nu_2^4 \leftarrow 0$	10367.184	0.398	1.019	−0.031	−0.004
$^{n}R(3,3)$	$4\nu_2^4 \leftarrow 0$	10454.539	0.530	0.871	−0.188	−0.162
$P(4,3)$	$5\nu_2^1 \leftarrow 0$	10624.888	0.052	1.003	−0.073	−0.080
$P(4,4)$	$5\nu_2^1 \leftarrow 0$	10632.042	0.298	0.911	−0.166	−0.172
$P(3,2)$	$5\nu_2^1 \leftarrow 0$	10705.894	−0.029	0.995	−0.090	−0.092
$Q(4,3)^{u}$	$5\nu_2^1 \leftarrow 0$	10710.311	0.203	0.912	−0.173	−0.188
$P(3,3)$	$5\nu_2^1 \leftarrow 0$	10730.107	−0.007	1.146	0.060	0.058
$P(2,2)$	$5\nu_2^1 \leftarrow 0$	10752.369	−0.099	1.057	−0.032	−0.035
$P(2,1)$	$5\nu_2^1 \leftarrow 0$	10766.320	0.008	1.069	−0.021	−0.022
$Q(3,2)^{u}$	$5\nu_2^1 \leftarrow 0$	10779.136	1.165	0.556	−0.536	−0.544
$P(3,0)$	$5\nu_2^1 \leftarrow 0$	10798.691	0.229	1.042	−0.050	−0.045
$P(1,1)$	$5\nu_2^1 \leftarrow 0$	10798.785	−0.253	1.039	−0.054	−0.057
$P(5,3)^{l}$	$5\nu_2^1 \leftarrow 0$	10811.027	0.568	1.105	0.011	0.026
$P(3,1)^{u}$	$5\nu_2^1 \leftarrow 0$	10813.699	0.235	1.110	0.016	0.023
$Q(1,0)$	$5\nu_2^1 \leftarrow 0$	10831.677	−0.186	1.011	−0.085	−0.089
$Q(4,2)^{u}$	$5\nu_2^1 \leftarrow 0$	10855.172	0.259	1.050	−0.049	−0.050
$Q(3,0)$	$5\nu_2^1 \leftarrow 0$	10935.631	−0.005	0.843	−0.263	−0.257
$Q(1,1)$	$5\nu_2^1 \leftarrow 0$	10939.559	0.003	1.071	−0.037	−0.029
$Q(2,2)$	$5\nu_2^1 \leftarrow 0$	10964.605	−0.017	1.017	−0.094	−0.083
$^{+6}R(2,2)$	$5\nu_2^1 \leftarrow 0$	10964.792	0.284	0.911	−0.199	−0.198
$Q(3,3)$	$5\nu_2^1 \leftarrow 0$	10968.257	0.052	1.017	−0.093	−0.083
$R(1,1)^{l}$	$5\nu_2^1 \leftarrow 0$	11044.146	0.175	1.001	−0.118	−0.107
$R(3,3)^{u}$	$5\nu_2^1 \leftarrow 0$	11053.686	0.197	0.920	−0.199	−0.196
$Q(2,1)^{u}$	$5\nu_2^1 \leftarrow 0$	11071.117	0.229	1.115	−0.005	0.015
$R(3,2)^{u}$	$5\nu_2^1 \leftarrow 0$	11195.625	0.260	1.066	−0.068	−0.050
$R(1,0)$	$5\nu_2^1 \leftarrow 0$	11228.601	0.243	1.074	−0.062	−0.034
$R(1,1)^{u}$	$5\nu_2^1 \leftarrow 0$	11244.353	0.226	1.120	−0.018	0.012
$R(2,1)^{l}$	$5\nu_2^1 \leftarrow 0$	11246.707	0.359	1.001	−0.138	−0.111
$R(2,2)^{l}$	$5\nu_2^1 \leftarrow 0$	11304.480	0.294	1.015	−0.129	−0.097
$^{-6}P(5,5)^{u}$	$5\nu_2^1 \leftarrow 0$	11422.627	0.938	0.474	−0.683	−0.611
$R(2,1)^{u}$	$5\nu_2^1 \leftarrow 0$	11496.796	0.450	1.213	0.049	0.101
$R(3,3)^{l}$	$5\nu_2^1 \leftarrow 0$	11576.154	0.578	1.150	−0.022	0.034
$R(3,0)$	$5\nu_2^1 \leftarrow 0$	11618.521	0.609	1.675	0.499	0.559
$^{+6}Q(3,0)$	$5\nu_2^3 \leftarrow 0$	10657.149	0.018	0.937	−0.142	−0.161
$^{+6}Q(2,1)$	$5\nu_2^3 \leftarrow 0$	10789.844	−0.180	0.981	−0.112	−0.119
$^{+6}Q(3,1)$	$5\nu_2^3 \leftarrow 0$	10803.820	0.052	0.955	−0.139	−0.145
$^{+6}Q(4,1)$	$5\nu_2^3 \leftarrow 0$	10816.758	0.149	1.034	−0.060	−0.066
$^{+6}R(1,1)$	$5\nu_2^3 \leftarrow 0$	10963.072	−0.175	0.994	−0.117	−0.115
$^{-6}P(4,4)$	$5\nu_2^3 \leftarrow 0$	11482.938	0.833	0.690	−0.473	−0.402
$P(3,3)$	$5\nu_2^3 \leftarrow 0$	11496.055	−0.434	0.542	−0.622	−0.552
$^{+6}R(3,2)$	$5\nu_2^3 \leftarrow 0$	11515.921	0.474	1.029	−0.137	−0.091
$Q(3,0)$	$5\nu_2^3 \leftarrow 0$	11691.577	1.012	0.680	−0.503	−0.426
$Q(2,2)$	$5\nu_2^3 \leftarrow 0$	11788.272	1.014	0.570	−0.624	−0.536
$R(3,3)$	$5\nu_2^3 \leftarrow 0$	11953.935	0.704	0.705	−0.505	−0.417
$P(4,3)$	$5\nu_2^5 \leftarrow 0$	11494.835	2.287	1.695	0.531	0.531
$^{+6}Q(3,1)$	$5\nu_2^5 \leftarrow 0$	11564.098	1.044	0.902	−0.269	−0.273
$P(3,3)$	$5\nu_2^5 \leftarrow 0$	11571.876	0.889	0.826	−0.346	−0.342
$^{+6}P(2,2)$	$5\nu_2^5 \leftarrow 0$	11578.494	0.866	0.619	−0.553	−0.550
$^{+6}Q(1,0)$	$5\nu_2^5 \leftarrow 0$	11606.157	0.901	0.833	−0.341	−0.339
$^{+6}R(2,2)$	$5\nu_2^5 \leftarrow 0$	11694.789	1.003	1.226	0.042	0.042
$^{+6}R(1,1)$	$5\nu_2^5 \leftarrow 0$	11707.268	1.004	1.022	−0.163	−0.161
$^{+6}Q(1,1)$	$5\nu_2^5 \leftarrow 0$	11707.801	1.054	0.760	−0.426	−0.415
$^{+6}R(3,1)$	$5\nu_2^5 \leftarrow 0$	11728.382	0.562	1.385	0.198	0.197
$^{+6}R(3,2)$	$5\nu_2^5 \leftarrow 0$	11793.656	0.825	1.031	−0.163	−0.157
$^{+6}R(3,0)$	$5\nu_2^5 \leftarrow 0$	11835.025	0.807	1.102	−0.095	−0.086
$Q(3,3)$	$5\nu_2^5 \leftarrow 0$	11839.565	0.925	0.348	−0.850	−0.832
$^{+6}R(1,0)$	$5\nu_2^5 \leftarrow 0$	11854.459	1.267	1.012	−0.188	−0.168
$R(3,3)$	$5\nu_2^5 \leftarrow 0$	12320.975	1.158	0.719	−0.529	−0.478
$^{t}Q(1,0)$	$6\nu_2^2 \leftarrow 0$	12419.140	0.172	0.533	−0.724	−0.726
$^{t}Q(3,0)$	$\nu_1 + 4\nu_2^0 \leftarrow 0$	11562.798	0.758	0.388	−0.782	−0.804
$^{t}R(3,0)$	$\nu_1 + 4\nu_2^0 \leftarrow 0$	11978.640	0.994	0.526	−0.686	−0.682
$^{n}R(2,2)$	$\nu_1 + 4\nu_2^0 \leftarrow 0$	12097.708	0.967	0.665	−0.560	−0.545
$^{t}R(3,3)$	$\nu_1 + 4\nu_2^2 \leftarrow 0$	12102.469	0.039	0.565	−0.660	−0.670
$^{t}R(1,0)$	$\nu_1 + 4\nu_2^2 \leftarrow 0$	12246.368	0.841	0.384	−0.856	−0.843
$^{n}Q(4,3)$	$\nu_1 + 4\nu_2^2 \leftarrow 0$	12314.977	0.581	0.451	−0.797	−0.776
$^{n}R(3,3)$	$\nu_1 + 4\nu_2^2 \leftarrow 0$	12658.335	0.592	0.476	−0.806	−0.767
$^{t}P(4,3)$	$\nu_1 + 4\nu_2^4 \leftarrow 0$	12181.941	0.778	0.583	−0.651	−0.660
$^{t}Q(3,3)$	$\nu_1 + 4\nu_2^4 \leftarrow 0$	12525.302	0.785	0.605	−0.663	−0.654
$^{t}Q(1,1)$	$\nu_1 + 4\nu_2^4 \leftarrow 0$	12623.171	0.787	0.703	−0.575	−0.556
$^{t}R(1,0)$	$\nu_1 + 4\nu_2^4 \leftarrow 0$	12897.888	2.189	0.407	−0.899	−0.860
$^{n}R(4,3)$	$2\nu_1 + 2\nu_2^0 \leftarrow 0$	11114.428	1.193	0.520	−0.606	−0.577
$^{t}P(3,0)$	$2\nu_1 + 2\nu_2^2 \leftarrow 0$	10322.235	1.259	0.478	−0.566	−0.583
$^{t}Q(2,1)$	$2\nu_1 + 2\nu_2^2 \leftarrow 0$	10467.800	1.266	0.528	−0.532	−0.546
$^{t}Q(3,1)$	$2\nu_1 + 2\nu_2^2 \leftarrow 0$	10468.544	1.248	0.522	−0.538	−0.552

Table 3 (*continued*)

Assignment	Band	Observed (cm^{-1})	ΔNMT (cm^{-1})	ΔSAH $E^{(0)}$ (cm^{-1})	ΔSAH $E^{(4)}$ (cm^{-1})	ΔSAH $E^{(2)}$ (cm^{-1})
$^{n}P(2,1)$	$2v_1+2v_2^2\leftarrow 0$	10496.571	1.336	0.437	−0.625	−0.631
$^{t}R(4,4)$	$2v_1+2v_2^2\leftarrow 0$	10497.078	1.146	0.560	−0.504	−0.534
$^{n}P(3,2)$	$2v_1+2v_2^2\leftarrow 0$	10507.396	1.351	0.384	−0.680	−0.683
$^{n}P(4,3)$	$2v_1+2v_2^2\leftarrow 0$	10528.992	1.421	0.393	−0.673	−0.672
$^{n}P(5,5)^{l}$	$2v_1+2v_2^2\leftarrow 0$	10558.882	1.002	0.650	−0.419	−0.411
$^{t}Q(3,0)$	$2v_1+2v_2^2\leftarrow 0$	10560.443	1.284	0.457	−0.611	−0.617
$^{t}Q(1,0)$	$2v_1+2v_2^2\leftarrow 0$	10568.209	1.299	0.471	−0.599	−0.603
$^{n}P(1,1)$	$2v_1+2v_2^2\leftarrow 0$	10581.256	1.326	0.427	−0.645	−0.645
$^{n}P(3,3)$	$2v_1+2v_2^2\leftarrow 0$	10583.688	1.409	0.313	−0.758	−0.756
$^{n}P(2,2)$	$2v_1+2v_2^2\leftarrow 0$	10586.424	1.370	0.377	−0.695	−0.694
$^{t}R(3,3)$	$2v_1+2v_2^2\leftarrow 0$	10609.077	1.161	0.852	−0.222	−0.238
$^{t}R(2,2)$	$2v_1+2v_2^2\leftarrow 0$	10621.634	1.259	0.630	−0.445	−0.456
$^{t}R(1,1)$	$2v_1+2v_2^2\leftarrow 0$	10641.024	1.276	0.545	−0.533	−0.537
$^{n}Q(1,1)$	$2v_1+2v_2^2\leftarrow 0$	10669.815	1.325	0.434	−0.646	−0.642
$^{n}Q(2,1)$	$2v_1+2v_2^2\leftarrow 0$	10671.864	1.301	0.437	−0.644	−0.639
$^{n}P(4,4)^{u}$	$2v_1+2v_2^2\leftarrow 0$	10686.611	0.208	0.922	−0.161	−0.143
$^{t}R(4,3)$	$2v_1+2v_2^2\leftarrow 0$	10690.240	1.116	0.840	−0.243	−0.254
$^{t}R(3,2)$	$2v_1+2v_2^2\leftarrow 0$	10705.364	0.961	0.413	−0.671	−0.677
$^{t}R(2,1)$	$2v_1+2v_2^2\leftarrow 0$	10725.953	1.251	0.536	−0.550	−0.550
$^{t}R(1,0)$	$2v_1+2v_2^2\leftarrow 0$	10752.150	1.267	0.505	−0.583	−0.577
$^{n}Q(3,2)^{u}$	$2v_1+2v_2^2\leftarrow 0$	10760.627	0.206	0.923	−0.167	−0.156
$^{n}Q(2,2)$	$2v_1+2v_2^2\leftarrow 0$	10766.108	1.362	0.405	−0.685	−0.674
$^{n}Q(4,2)^{u}$	$2v_1+2v_2^2\leftarrow 0$	10793.060	1.278	0.524	−0.569	−0.555
$^{t}R(3,1)$	$2v_1+2v_2^2\leftarrow 0$	10805.800	1.206	0.516	−0.578	−0.574
$^{n}R(1,1)$	$2v_1+2v_2^2\leftarrow 0$	10845.089	1.309	0.453	−0.646	−0.631
$^{n}Q(4,3)$	$2v_1+2v_2^2\leftarrow 0$	10847.551	1.457	0.481	−0.618	−0.601
$^{n}R(2,1)$	$2v_1+2v_2^2\leftarrow 0$	10934.327	1.318	0.453	−0.654	−0.636
$^{t}R(3,0)$	$2v_1+2v_2^2\leftarrow 0$	10935.358	1.520	0.776	−0.330	−0.314
$^{n}R(2,2)^{u}$	$2v_1+2v_2^2\leftarrow 0$	11019.351	0.205	0.932	−0.184	−0.159
$^{n}R(3,1)^{u}$	$2v_1+2v_2^2\leftarrow 0$	11024.705	1.991	1.138	0.022	0.045
$Q(2,1)^{l}$	$2v_1+3v_2^1\leftarrow 0$	12207.905	0.567	0.150	−1.086	−1.096
$P(2,2)$	$2v_1+3v_2^1\leftarrow 0$	12222.032	−0.159	0.494	−0.744	−0.743
$P(3,3)$	$2v_1+3v_2^1\leftarrow 0$	12246.574	0.801	0.499	−0.740	−0.734
$Q(1,0)$	$2v_1+3v_2^1\leftarrow 0$	12253.670	0.399	0.374	−0.866	−0.872
$P(6,6)$	$3v_1+v_2^1\leftarrow 0$	10874.681	2.113	0.945	−0.156	−0.177
$P(5,5)$	$3v_1+v_2^1\leftarrow 0$	10953.026	2.122	1.173	0.064	0.047
$P(4,3)$	$3v_1+v_2^1\leftarrow 0$	11015.488	1.591	0.703	−0.413	−0.427
$P(4,4)$	$3v_1+v_2^1\leftarrow 0$	11033.268	1.627	0.729	−0.389	−0.401
$P(3,3)$	$3v_1+v_2^1\leftarrow 0$	11111.798	1.587	0.697	−0.428	−0.437
$Q(3,0)$	$3v_1+v_2^1\leftarrow 0$	11278.517	1.634	0.641	−0.500	−0.505
$Q(1,0)$	$3v_1+v_2^1\leftarrow 0$	11318.080	1.631	0.616	−0.530	−0.530
$Q(3,3)$	$3v_1+v_2^1\leftarrow 0$	11358.855	1.593	0.719	−0.431	−0.427
$R(1,0)$	$3v_1+v_2^1\leftarrow 0$	11503.614	1.611	0.646	−0.518	−0.508
$R(3,3)^{u}$	$3v_1+v_2^1\leftarrow 0$	11668.916	0.296	0.845	−0.336	−0.318
$^{-6}R(4,4)^{l}$	$3v_1+v_2^1\leftarrow 0$	11892.128	1.114	0.566	−0.639	−0.603
$R(2,0)$	Unknown$\leftarrow v_2^1$	10827.764	0.744	0.617	−0.479	–
$R(2,3)$	Unknown$\leftarrow v_2^1$	11265.189	3.200	2.584	1.444	–
$R(6,6)$	Unknown	10329.307	1.069	0.937	−0.108	–
$P(6,6)$	Unknown	10462.405	0.250	1.019	−0.040	–
$R(5,5)$	Unknown	10496.287	1.437	0.616	−0.446	–
$R(4,3)$	Unknown	10573.997	0.591	0.820	−0.251	–
$Q(5,0)$	Unknown	10639.058	0.155	0.883	−0.194	–
$Q(5,3)$	Unknown	10666.604	0.318	0.809	−0.271	–
$R(6,6)$	Unknown	11036.111	1.518	0.847	−0.270	–
$R(5,5)$	Unknown	11046.569	0.681	0.918	−0.200	–
$R(4,4)$	Unknown	11048.996	0.557	0.819	−0.300	–
$R(5,0)$	Unknown	11114.628	1.376	0.535	−0.589	–
$P(6,6)$	Unknown	11331.112	1.103	0.251	−0.896	–
$R(4,3)$	Unknown	11556.914	0.672	0.849	−0.322	–
$P(6,6)$	Unknown	11947.074	0.205	0.086	−1.123	–
$Q(3,0)$	Unknown	12116.353	−1.290	−0.035	−1.261	–
$R(4,3)$	Unknown	12331.180	0.895	0.593	−0.657	–
$P(3,3)$	Unknown	12502.614	0.436	0.987	−0.279	–
$R(3,0)$	Unknown	12536.621	1.155	0.522	−0.747	–
$R(1,0)$	Unknown	13056.013	0.618	0.481	−0.841	–
$Q(1,0)$	Unknown	13597.367	0.618	0.122	−1.255	–
$R(3,3)$	Unknown	13606.093	0.749	0.028	−1.349	–
$Q(1,0)$	Unknown	13676.446	−2.211	−0.837	−2.221	–

duction of rotational magnetic moments. Using a Hamiltonian containing rotational and magnetic energy terms in which the contribution of electrons are explicitly given, Oka and Morino [54] derived a relation between the non-adiabatic correction on the moment of inertia and rotational magnetic moments as

$$(\Delta I_{\alpha\alpha})_{\text{non-adiabatic}} = -\frac{m}{M} g_{\alpha\alpha} I_{\alpha\alpha} \tag{6}$$

Table 4
Average discrepancies between experiment and theory in cm^{-1} for each band.

Band	Total Lines	$\overline{\Delta NMT}$	$\overline{\Delta SAH\ E^{(0)}}$	$\overline{\Delta SAH\ E^{(4)}}$	$\overline{\Delta SAH\ E^{(2)}}$
$4\nu_2^4 \leftarrow 0$	3	0.47 ± 0.07	0.97 ± 0.08	−0.09 ± 0.09	−0.06 ± 0.09
$5\nu_2^1 \leftarrow 0$	31	0.24 ± 0.30	1.02 ± 0.19	−0.09 ± 0.19	−0.08 ± 0.19
$5\nu_2^3 \leftarrow 0$	11	0.32 ± 0.52	0.83 ± 0.19	−0.31 ± 0.23	−0.27 ± 0.19
$5\nu_2^5 \leftarrow 0$	14	1.04 ± 0.40	0.96 ± 0.33	−0.23 ± 0.34	−0.22 ± 0.33
$6\nu_2^2 \leftarrow 0$	1	−0.17	0.53	−0.72	−0.73
$\nu_1 + 4\nu_2^0 \leftarrow 0$	3	0.91 ± 0.13	0.53 ± 0.14	−0.68 ± 0.11	−0.68 ± 0.13
$\nu_1 + 4\nu_2^2 \leftarrow 0$	4	0.51 ± 0.34	0.47 ± 0.08	−0.78 ± 0.08	−0.76 ± 0.07
$\nu_1 + 4\nu_2^4 \leftarrow 0$	4	1.13 ± 0.75	0.57 ± 0.11	−0.70 ± 0.12	−0.69 ± 0.11
$2\nu_1 + 2\nu_2^0 \leftarrow 0$	1	−1.19	0.52	−0.61	−0.58
$2\nu_1 + 2\nu_2^2 \leftarrow 0$	28	1.28 ± 0.12	0.51 ± 0.13	−0.57 ± 0.13	−0.57 ± 0.13
$2\nu_1 + 2\nu_2^2 \leftarrow 0$[a]	5	0.78 ± 0.82	0.89 ± 0.22	−0.21 ± 0.22	−0.19 ± 0.22
$2\nu_1 + 3\nu_2^1 \leftarrow 0$	4	0.40 ± 0.41	0.38 ± 0.16	−0.86 ± 0.16	−0.86 ± 0.17
$3\nu_1 + \nu_2^1 \leftarrow 0$	11	1.54 ± 0.49	0.75 ± 0.17	−0.39 ± 0.19	−0.39 ± 0.18
Unknown	23	0.65 ± 1.00	0.63 ± 0.61	−0.55 ± 0.68	–
Total	143	0.77 ± 0.68	0.75 ± 0.36	−0.39 ± 0.39	−0.35 ± 0.31

[a] These were from the *u* transitions and were consistently different from the other $2\nu_1 + 2\nu_2^2 \leftarrow 0$ transitions. The reason is not clear.

where m and M are the mass of the electron and proton, respectively, $I_{\alpha\alpha}$ are the moments of inertia along the α-axis ($\alpha = a,b,c$) and $g_{\alpha\alpha}$ are the diagonal elements of the g tensor for rotational magnetic moment.

Using theoretical values of $g_{\alpha\alpha}$ given by Oddershede and Sabin [55]

$$g_{aa} = g_{bb} = -0.068 \text{ and } g_{cc} = -0.021 \tag{7}$$

and the H_3^+ rotational constants B = 43.568 cm^{-1} and C = 20.708 cm^{-1} [21] give

$$\bar{a}_1 = -(\Delta B)_{\text{non-adiabatic}} = -\frac{m}{M} g_{bb} B = 1.62 \times 10^{-3} \text{cm}^{-1} \tag{8}$$

$$\bar{a}_2 = -(\Delta C - \Delta B)_{\text{non-adiabatic}} = -\frac{m}{M}(g_{cc} C - g_{bb} B) = -1.38 \times 10^{-3} \text{cm}^{-1} \tag{9}$$

which agrees reasonably well with the value of SAH [53], that is $\bar{a}_1 = 2.04 \times 10^{-3} \text{cm}^{-1}$ and $\bar{a}_2 = -1.36 \times 10^{-3} \text{cm}^{-1}$.

Recently developed methods of ultrahigh resolution molecular ion spectroscopy by Schiller and colleagues [56] using sympathetic cooling may open the door for Zeeman effect measurements of molecular ions. Measurements of the rotational magnetic moment for H_3^+ are awaited.

Averaged discrepancies between the observed and calculated values for each band are summarized in Table 4. As expected the errors become larger at higher energies. Certain trends also become apparent when the individual bands are examined. Theory does compare well with experiment with the errors typically within a wavenumber, but there is a systematic trend for the different bands.

While the strongest transitions have been recorded, there still exists hundreds of weaker transitions in this region that are below our sensitivity and have not been observed. Additionally there still exists the region above ~14000 cm^{-1} to the predissociation spectrum region around 35000 cm^{-1} which was first recorded by Carrington in 1982 [57]. These spectrum remains completely unassigned, in spite of much theoretical work [58]. The new method by Kreckel et al. [47] may reach such a high energy.

Acknowledgments

The authors wish to thank J.K.G. Watson for sending us the results of his calculations and C.F. Neese for his assistance in improving the laser spectrometer and its control software. This work was supported by NSF Grant PHYS-03-54200.

References

[1] W. Heitler, F. London, Z. Physik 44 (1927) 455–471.
[2] H.M. James, A.S. Coolidge, J. Chem. Phys. 1 (1933) 825–835.
[3] A.S. Coolidge, H.M. James, J. Chem. Phys. 6 (1938) 730–734.
[4] G. Herzberg, Trans. Roy. Soc. Can. 5 (Ser. IV) (1967) 3–36.
[5] G. Herzberg, Trans. Roy. Soc. Can. 10 (Ser. IV) (1982) 151–178.
[6] W. Kołos, L. Wolniewicz, J. Mol. Spectrosc. 54 (1975) 303–311.
[7] D.M. Bishop, L.M. Cheung, J. Mol. Spectrosc. 75 (1979) 462–473.
[8] J.J. Thomson, Phil. Mag. 21 (1911) 225–249.
[9] N. Bohr, Nobelinst. Meddel. 5 (1919) 1–16.
[10] H.S.W. Massey, Proc. Cambridge Philos. Soc. 27 (1931) 451–459.
[11] J. Hirschfelder, Dissertation, Prinston University, 1935.
[12] J. Hirschfelder, H. Eyring, N. Rosen, J. Chem. Phys. 4 (1936) 130–133.
[13] J. Hirschfelder, H. Diamond, H. Eyring, J. Chem. Phys. 5 (1937) 695–703.
[14] D. Stevenson, J. Hirschfelder, J. Chem. Phys. 5 (1937) 933–940.
[15] J.O. Hirschfelder, J. Chem. Phys. 6 (1938) 795–806.
[16] C.A. Coulson, Proc. Cambridge Philos. Soc. 31 (1935) 244–257.
[17] T. Oka, Molecular Ions: Spectroscopy, Structure and Chemistry, in: T.A. Miller, V.E. Bondybey (Eds.), North-Holland Publishing Co., Amsterdam, 1983, pp. 73–90.
[18] I.R. McNab, Adv. Chem. Phys. 89 (1995) 1–87.
[19] J.B. Anderson, J. Chem. Phys. 96 (1992) 3702–3706.
[20] G.D. Carney, R.N. Porter, J. Chem. Phys. 65 (1976) 3547–3565.
[21] T. Oka, Phys. Rev. Lett. 45 (1980) 531–534.
[22] J.K.G. Watson, J. Mol. Spectrosc. 103 (1984) 350–363.
[23] J. Tennyson, B.T. Sutcliffe, Mol. Phys. 51 (1984) 887–906.
[24] J. Tennyson, B.T. Sutcliffe, J. Chem. Soc. Faraday Trans. 2 82 (1986) 1151–1162.
[25] S. Miller, J. Tennyson, J. Mol. Spectrosc. 126 (1987) 183–192.
[26] S. Miller, J. Tennyson, J. Mol. Spectrosc. 128 (1988) 530–539.
[27] S. Miller, J. Tennyson, J. Mol. Spectrosc. 136 (1989) 223–240.
[28] W. Meyer, P. Botschwina, P. Burton, J. Chem. Phys. 84 (1986) 891–900.
[29] P. Drossart, J.P. Maillard, J. Caldwell, S.J. Kim, J.K.G. Watson, W.A. Majewski, J. Tennyson, S. Miller, S.K. Atreya, J.T. Clarke, J.H. Waite, R. Wagener, Nature 340 (1989) 539–541.
[30] M.G. Bawendi, B.D. Rehfuss, T. Oka, J. Chem. Phys. 93 (1990) 6200–6209.
[31] W.A. Majewski, P.A. Feldman, J.K.G. Watson, S. Miller, J. Tennyson, Astrophys. J. 347 (1989) L51–L54.
[32] L.-W. Xu, M. Rösslein, C.M. Gabrys, T. Oka, J. Mol. Spectrosc. 153 (1992) 726–737.
[33] L. Neale, S. Miller, J. Tennyson, Astrophys. J. 464 (1996) 516–520.
[34] R.M. Whitnell, J.C. Light, J. Chem. Phys. 90 (1989) 1774–1786.
[35] L. Wolniewicz, J. Hinze, J. Chem. Phys. 101 (1994) 9817–9829.
[36] J.K.G. Watson, Can. J. Phys. 72 (1994) 702–713.
[37] C.M. Lindsay, B.J. McCall, J. Mol. Spectrosc. 210 (2001) 60–83.
[38] W. Cencek, J. Rychlewski, R. Jaquet, W. Kutzelnigg, J. Chem. Phys. 108 (1998) 2831–2836.
[39] W. Kutzelnigg, R. Jaquet, Phil. Trans. R. Soc. A 364 (2006) 2855–2876.
[40] O.L. Polyansky, J. Tennyson, J. Chem. Phys. 110 (1999) 5056–5064.
[41] J. Tennyson, P. Barletta, M.A. Kostin, O.L. Polyansky, N.F. Zobov, Spectrochim. Acta, Part A 58 (2002) 663–672.
[42] P. Schiffels, A. Alijah, J. Hinze, Mol. Phys. 101 (2003) 189–209.
[43] A. Alijah, J. Hinze, Phil. Trans. R. Soc. A 364 (2006) 2877–2888.
[44] L. Velilla, B. Lepetit, A. Aguado, J.A. Beswick, M. Paniagua, J. Chem. Phys. 129 (2008) 084307.
[45] B.J. McCall, T. Oka, J. Chem. Phys. 113 (2000) 3104–3110.
[46] J.L. Gottfried, B.J. McCall, T. Oka, J. Chem. Phys. 118 (2003) 10890–10899.

[47] H. Kreckel, D. Bing, S. Reinhardt, A. Petrignani, M. Berg, A. Wolf, J. Chem. Phys. 129 (2008) 164312.
[48] S. Schlemmer, T. Kuhn, E. Lescop, D. Gerlich, Int. J. Mass Spectrom. 185 (1999) 589–602.
[49] J.T. Hougen, J. Chem. Phys. 37 (1962) 1433–1441.
[50] J.K.G. Watson, private communication (2002).
[51] J. Gottfried, Phil. Trans. R. Soc. A 364 (2006) 2917–2929.
[52] D. Uy, C.M. Gabrys, M.F. Jagod, T. Oka, J. Chem. Phys. 100 (1994) 6267–6274.
[53] P. Schiffels, A. Alijah, J. Hinze, Mol. Phys. 101 (2003) 175–188.
[54] T. Oka, Y. Morino, J. Mol. Spectrosc. 6 (1961) 472–482.
[55] J. Oddershede, J.R. Sabin, Chem. Phys. 122 (1988) 291–296.
[56] B. Roth, J.C.J. Koelemeij, H. Daerr, S. Schiller, Phys. Rev. A 74 (2006) 040501(R).
[57] A. Carrington, J. Buttenshaw, R.A. Kenndey, Mol. Phys. 45 (1982) 753–758.
[58] M.A. Kostin, O.L. Polyansky, J. Tennyson, H.Y. Mussa, J. Chem. Phys. 118 (2003) 3538–3542.